A Miniaturized Force Sensor Based on Hair-Like Flexible Magnetized Cylinders Deposited Over a Giant Magnetoresistive Sensor

Pedro Ribeiro[1,2], Mohammed Asadullah Khan[3], Ahmed Alfadhel[3], Jürgen Kosel[3], Fernando Franco[1,2], Susana Cardoso[1,2], Alexandre Bernardino[4], José Santos-Victor[4], and Lorenzo Jamone[5,4]

[1]INESC-Microssistemas e Nanotecnologias and IN, 1000-029 Lisbon, Portugal
[2]Physics Department, Instituto Superior Técnico, 1049-001 Lisbon, Portugal
[3]Computer, Electrical and Mathematical Sciences and Engineering Division, King Abdullah University of Science and Technology, Thuwal 23955-6900, Saudi Arabia
[4]Instituto de Sistemas e Robótica, Instituto Superior Técnico, 1049-001 Lisbon, Portugal
[5]Advanced Robotic at Queen Mary, School of Electronic Engineer and Computer Science, Queen Mary University of London, London E1 4NS, U.K.

The detection of force with higher resolution than observed in humans (∼1 mN) is of great interest for emerging technologies, especially surgical robots, since this level of resolution could allow these devices to operate in extremely sensitive environments without harming these. In this paper, we present a force sensor fabricated with a miniaturized footprint (9 mm^2), based on the detection of the magnetic field generated by magnetized flexible pillars over a giant magnetoresistive sensor. When these flexible pillars deflect due to external loads, the stray field emitted by these will change, thus varying the GMR sensor resistance. A sensor with an array of five pillars with 200 μm diameter and 1 mm height was fabricated, achieving a 0 to 26 mN measurement range and capable of detecting a minimum force feature of 630 μN. A simulation model to predict the distribution of magnetic field generated by the flexible pillars on the sensitive area of the GMR sensor in function of the applied force was developed and validated against the experimental results reported in this paper. The sensor was finally tested as a texture classification system, with the ability of differentiating between four distinct surfaces varying between 0 and 162 μm root mean square surface roughness.

Index Terms—**Force sensors, magnetic sensors, microsensors.**

I. Introduction

With the growing interest in humanoid and surgical robots, as well as tactile skins, the detection of forces with high precision and distributed in various points with small footprints (in the order of mm^2) has become of great interest, as it could allow these devices to operate safely in highly uncertain and sensitive environments [1], [2]. In recent years, many technologies have been developed to allow the detection of force with miniaturized footprint sensors, exploring a wide range of transduction media, e.g., piezoresistive [3], capacitive [4], piezoelectric [5], optical [6], [7], and magnetic [8]–[10].

Most of these sensors are optimized to work within the 1 mN to 10 N range, which is approximately the human tactile range, but increased sensitivity could provide robotic technologies with the capability to perform more delicate operations (for example, retinal surgery) [11].

One of the most sensitive tactile sensing structures found in nature is the ciliary structure. This structure is based on two organelles [12].

1) *Cilium:* A passive organelle, shaped as an elongated hair-like protuberance.
2) *Dendrite:* An active organelle, coupled to the cilium, capable of sensing electrical pulses whenever the cilium is actuated by and external force.

The first report in the literature of a sensor adapting the ciliary structure using flexible materials consisted of an array of polydimethylsiloxane (PDMS) cylinders in which living cells were deposited with the goal of determining cellular traction forces, which were measured by computing the deformation of the cylinders through image capture using a fast and high-resolution camera [13].

By embedding permanently magnetized material inside the PDMS structures, these elastic cylinders emit a stray magnetic field, which can be picked up by a sensor capable of detecting such field, and thus pillar deformation, directly associated with applied force, can be quantified by the magnitude of this field incident over the sensor, as reported in [14], where an elastomeric compound with embedded magnetic particles was deposited over a commercial magnetic field sensor as thin structures, mimicking cilia. However, this process only allowed control over the density of deposited micropillars. By microfabricating the artificial cilia, one can control the exact position, quantity, and shape of the pillars, granting a much higher level of sensor optimization. A sensor fabricated using this technique was initially used to measure fluid flows in microfluidic setups [15] and later as a proof-of-concept as force and tactile sensor [16].

Manuscript received March 10, 2017; revised April 21, 2017; accepted June 2, 2017. Date of publication June 13, 2017; date of current version October 24, 2017. Corresponding author: P. Ribeiro (e-mail: pedro.q.ribeiro@tecnico.ulisboa.pt).

Color versions of one or more of the figures in this paper are available online at http://ieeexplore.ieee.org.

Digital Object Identifier 10.1109/TMAG.2017.2714625

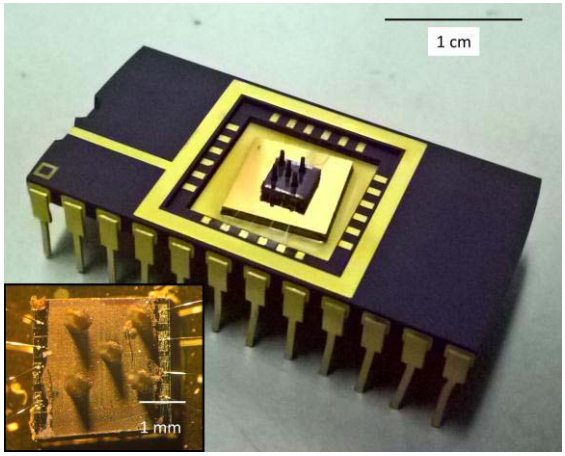

Fig. 1. Photograph of the finished tactile sensor, wirebonded to a chip carrier. Inset: Zoomed in view photograph of the wirebonded die. The clear appearance of the inset photograph is a result of the microscope illumination setup.

In this paper, we present a sensor with an area of 3×3 mm^2, capable of detecting a minimum force of 630 μN, as well as simulation results of the magnetic stray field generated by the magnetized cilia over the sensitive area (Fig. 1). In virtue of the high sensitivity achieved with the sensor, the detection of surface roughness is also tested and presented in the concluding section of this paper.

II. Fabricated Device

A sensor composed of an array of five micrometric magnetized cylinders with 200 μm nominal diameter and 1 mm height, composed of a PDMS using a 10:1 curing agent proportion with embedded NdFeB magnetic particles at a 14% v/v proportion expected to present a Young's Modulus of approximately 1 MPa, was deposited over a GMR sensor with two sensitive directions (with the X sensitive direction having 444 spin valves in series and the Y sensitive direction with 416 spin valves in series) and fabricated using a microfabrication process described in previous work [17]. It should be noted, however, that due to the Gaussian intensity profile of the CO2 laser cutting technique used to fabricate the mold for the pillars, these were wider in the bottom than at the top by 120 μm, assuming an approximately conical shape with 320 μm on the base and 200 μm, the nominal diameter, on the tip. In order to have simultaneous 2-D magnetic field detection, a top-pinned spin-valve stack (from bottom to top: Ta 10Å/NiFe 28Å/CoFe 23 Å/Cu 26 Å/CoFe 25Å/MnIr 80Å/Ta 30Å) [18], [19] was deposited for each sensitive direction, thus requiring no thermal treatment and facilitating the double sensitive direction fabrication process.

The die layout was designed with the intention of having X and Y sensitivity on the same areas while maximizing the area covered with active elements, with the magnetized flexible pillars placed at the extremities of the active area (one for each corner) and one in the center (five total). However, due to the high number of resistive elements in series, a detectable measurement for the sensors in both X and Y sensitive directions simultaneously could not be achieved, unless the sensor was fed an amount of power likely to damage it.

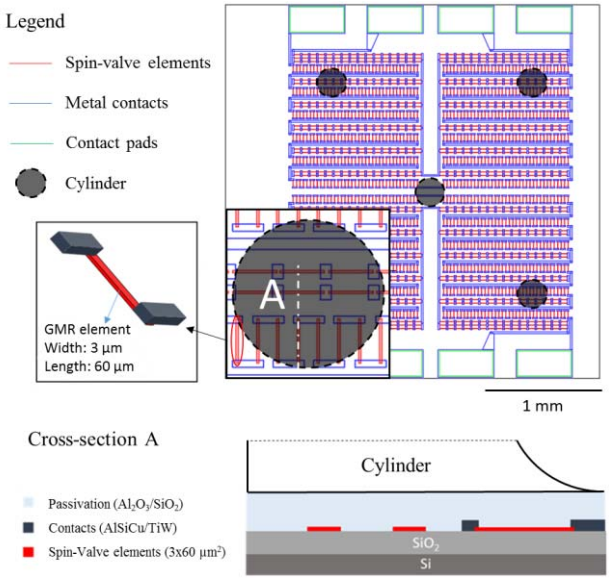

Fig. 2. Diagram of the fabricated GMR sensor die, with the micropillar positions. The red areas represent spin-valve sensors while blue areas represent metallic contacts. The black circles represent the positions over the die where the pillars were positioned. Bottom: Detail of cross Section A.

A diagram of the GMR sensor layout and the positioning of the magnetized cylinders is presented in Fig. 2.

III. Simulation

The response of the sensor is dependent of the two main constitutive elements of the sensor, the cilia and the GMR sensor, in which the deformation of the former imposes the magnetic field configuration incident over the sensor. Therefore, the main components that must be simulated are:

1) structural mechanics of the flexible magnetized pillars (that will predict the shape of the pillars in function of an arbitrary applied load);
2) the stray magnetic field generated by the deformed configuration and the shape and magnitude of this magnetic field over the spin-valve sensitive plane.

To accomplish the simulation of pillar deformation, an finite-element method (FEM) model was used, using the neo-Hookean model hyperelasticity model as constitutive model for the cilia [20].

From this deformation, ten points collinear with the undeformed pillar symmetry axis were selected to model its deformation for the next step of the model (calculating the magnetic field over the spin-valve area). In this step, each deformation point is approximated as a dipole with 1/10 of the magnetic moment of a single pillar. The magnetic field induced by each dipole of each pillar is calculated over a sensor area element, and finally all the contributions over each area element are added, thus yielding the magnetic field incident over the spin-valve area. In Fig. 3, the distributed magnetic field over a 3×3 mm^2 sensor, generated by an array of five pillars (equivalent to the diagram presented in Fig. 2) is presented. This case corresponds to a distribution of magnetic field caused by the cylinders with a deformation caused by a load magnitude of 15 mN applied in the direction perpendicular to the symmetry axis of the cylinder and concentrated in its tip.

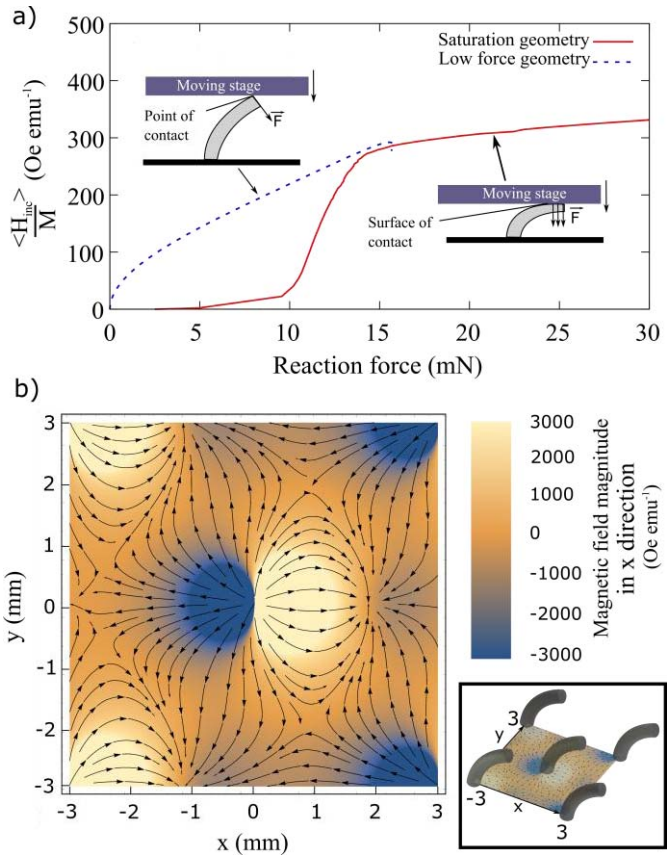

Fig. 3. (a) Stage reaction force versus average magnetic field over spin-valve plane. The two simulation geometries used for simulating the active region and the saturated region are presented, as well as the results of the simulation for each. (b) Density plot of the magnitude of the magnetic field emitted by five pillars with 1 mm height and 200 μm diameter on the x-direction. The arrows represent the stream lines of the projection of the magnetic field emitted by the deformed pillars over the sensitive plane. Inset: Distribution of the pillars over the sensitive plane.

The simulation was modeled in a two-configuration model, one of these to model the active response of the sensor, and another one to model the saturation region. While in the active region, the force driving the deformation results from a reaction force parallel to the pillar top plane. The sensor reaches saturation when most of the force starts being applied vertically and in the side wall of the cylinder, requiring a larger force to further deform the pillar since now this force is distributed over a surface that extends beyond the tip of the cylinder [Fig. 3(a)].

It can be noticed that the magnetic field is concentrated near the base of pillar, which is indicative that magnetic material embedded closer to the bottom of the pillar has a higher contribution to the spin-valve signal than magnetic material embedded closer to the tip, and thus, deformation on the bottom of the pillar should be more relevant than deformation at the top.

IV. Experimental Results

A. GMR Sensor Characterization

The magnetotransport curve of the deposited spin valves was measured using a setup consisting of two Helmholtz coils (that imposed a well-defined and uniform magnetic field for a certain current flow), between which the sample was placed. A constant current of 100 μA was fed to the sensor for each sensitive direction using a sourcemeter (Keithley 220) while the voltage was being monitored in the same terminals with a multimeter. All the instruments (multimeter, precision current source, and the current source for the coils) were connected via general purpose interface bus and controlled in real time, by simultaneously imposing a magnetic field, inducing a current in the sensor and measuring the voltage, for a magnetic field sweep from -140 to 140 Oe and back.

The magnetoresistances were determined as 5% and 4.40% with sensitivities of 146.6 and 118.8 Oe Ω^{-1} for the X and Y sensitive directions, respectively. The linear range of the GMR sensor is approximately between -25 and 37.5 Oe (62.5 Oe span), much higher than the maximum expected magnetic field to be generated by the flexible pillars (3 Oe). It should be noted that the difference in sensitivity for each sensitive direction stems from the difference in the spin-valve array length for each direction.

B. Force–Voltage Characterization and Simulation Fitting

The force characterization of the sensor was performed using a setup consisting of a motorized micropositioning setup to which the sensor, wirebonded to a chip carrier, was attached, and incrementally lowered over a precision balance (Precisa junior 60 A) to monitor the normal force exerted on the sensor [Fig. 4(a)], until the cylinders were completely deflected (with their side in contact with the substrate). The voltage in the terminals of the GMR sensor was measured using a multimeter (Hewlett–Packard 34401A) while power was provided by a precision current source (Keithley 2401). The system was controlled with a PC in real time, using a general-purpose interface bus connection, apart from the balance.

Because our FEM model is only capable of predicting deformations over the whole force domain for cylindrical structures, and the pillar is wider on the bottom than it is on top, pillar diameter, and magnetic moment, which is dependent on pillar volume, were left as free parameters. The other two known (and therefore fixed) pillar parameters were pillar height (1 mm) and Young's Modulus (1 MPa). The results of this test and the simulated fitting are presented in Fig. 4(b).

The magnetization of the pillar as well as its diameter was determined by fitting the simulation results to the experimentally obtained data, for which the best fitting values were 0.9 memu for the magnetic moment and 280 μm for the cylinder diameter. A vibrating sample magnetometer measurement of the cylinders constitutive material revealed these had a total magnetization of 2.8 memu, approximately 3 times larger than the value predicted by the experimental method. This discrepancy can be a consequence of the non-uniformity of the magnetic material inside the cylinder, the conical shape of the cylinder, and variations in spin-valve sensitivity from heating during operation. However, the method still predicted the behavior of the sensor correctly, and within the same order of magnitude of all cylinder parameters.

The minimum force feature measured was of 630 μN of magnitude.

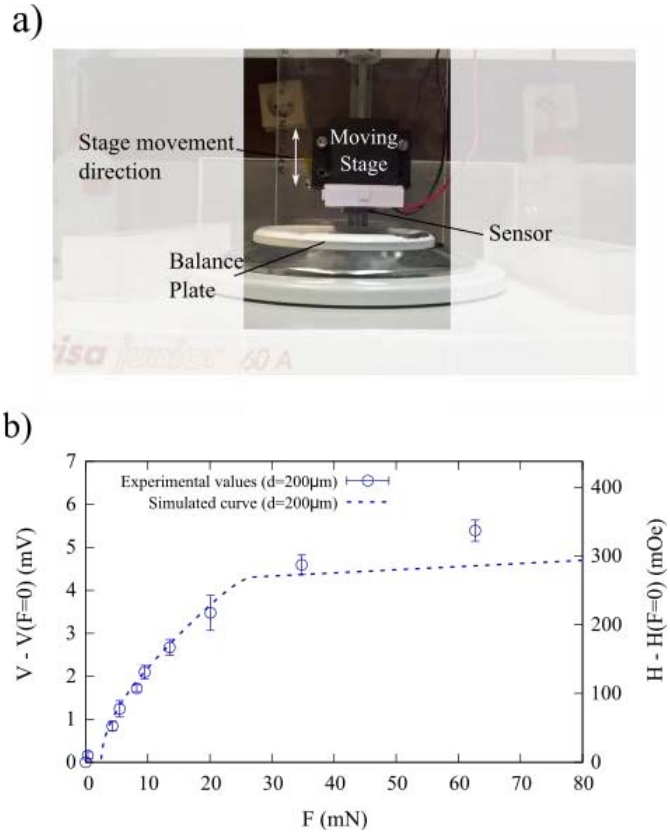

Fig. 4. (a) Experimental setup for force characterization. The stage moves vertically, while the balance detects the reaction force of the cylinders to deformation in the vertical direction. (b) Force characterization test results, and simulated curve using the experimental parameters and fit to magnetic moment and pillar diameter. The nominal diameter of the cylinder is presented in the legend, and the force presented is converted by the balance reading (the vertical component only).

C. Surface Roughness Detection

The capability of detecting surface roughness of a material was tested for the sensor using an operation current of 100 μA. For this test, a setup consisting of a Cartesian motor stage, capable of moving in X, Y, and Z was used, to which the sensor was fixed, while the tested material was fixed above the stage (and therefore the sensor) in such a way that the cilia would come in contact and brush against the material [Fig. 5(a)].

The tested materials were:

1) atomically flat silicon—0 μm surface roughness;
2) P1000, P320, and P100 grit sandpaper—18.3, 46.2, and 162 μm root mean square (rms) surface roughness respectively (according to International Organization for Standardization 6344).

In virtue of the silicon surface having no surface roughness, the rms voltage signal obtained for it represents the noise floor of texture detection, since the ac component of this signal should be null, and therefore, a higher signal that this one should be caused by the cilia movement due to the sandpaper roughness.

As expected, an increase in surface roughness lead to an increase in the rms signal measured, with the smoothest sandpaper generating a signal of 46.6 μV rms, above the

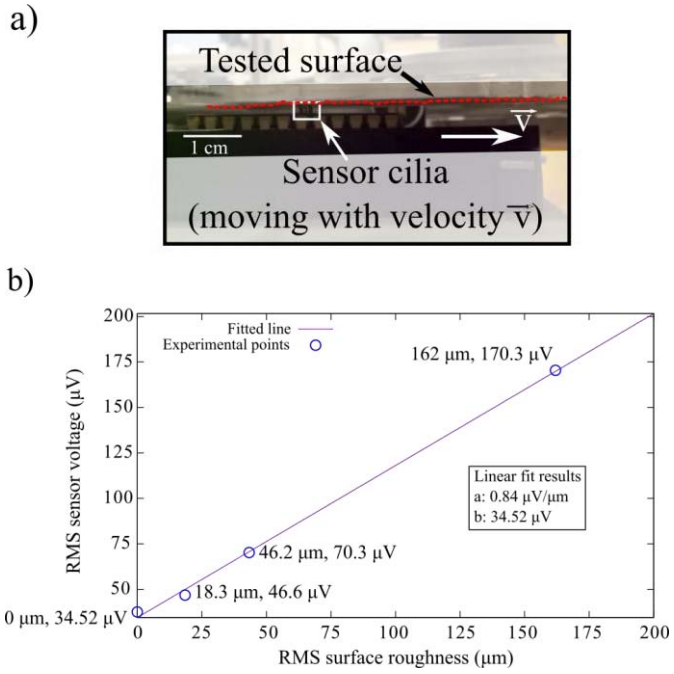

Fig. 5. (a) Photograph of the experimental setup. (b) Sensor voltage versus surface roughness, with linear fit.

37.6 μV rms noise floor, while the roughest generated a 170.3 μV rms signal.

The obtained results [Fig. 5(b)] showed a direct proportionality between surface roughness and measured voltage, and therefore, a linear fit of the data was performed, which revealed a 0.84 μV/μm constant of proportionality between the roughness of a surface and the rms of the ac signal component detected by the sensor. This quantity is directly related to the variation in deformation of the cylinders, as these overcome the uniformities of the tested surface during their movement as well as to the effective displacement of the pillar caused by the roughness on which the pillar is in contact with the textured surface. It should be noted that the velocity at which the measurement is performed can modify its outcome, especially if the measurement is performed too fast, since variations in surface roughness can be missed, especially when using a slow sampling rate (lower than 20 samples per second).

It should be noted that the noise floor in this test is much lower than the uncertainty obtained when measuring the experimental points for the force characterization test. This difference occurs because in this setup because both sensor and surface are fixed to an unmovable structure, while in the previous test, the cilia were in contact with the balance plate, which has freedom to rotate (as per balance design).

V. Conclusion

This paper was focused on the simulation and characterization of a sub-mN resolving force sensor.

A simulation model was presented, fitting well with the fabricated device force-electrical signal characteristic in terms of response behavior. However, the simulation did not predict perfectly the relation some of the fabricated devices parameters, namely, magnetic moment and diameter of the cylinders, despite having predicted a value within the same order of

magnitude of these, indicating that these differences could derive from non-idealities present in the real device that were assumed to be insignificant for the simulation, specifically, the non-uniformity of magnetic material inside the cylinders and variations on the sensitivity of the GMR sensor with temperature.

The sensor was finally tested as a surface roughness gauge, having revealed a linear correlation between the ac component of the measured signal and the surface roughness of the tested material, which is expected since for small variations of surface roughness, and thus, pillar deformation, only the first-order (linear) variations should be noticeable, with all higher orders being negligible.

ACKNOWLEDGMENT

This work was supported under Project EXCL/CTM-NAN/0441/2012, Project PTDC/CTM-NAN/3146/2014, and Project UID/EEA/50009/2013. The work of F. Franco was supported by FCT Project under Grant SFRH/BD/111538/2015. The work of L. Jamone was supported by LIMOMAN—PIEFGA-2013-628315.

REFERENCES

[1] M. I. Tiwana, S. J. Redmond, and N. H. Lovell, "A review of tactile sensing technologies with applications in biomedical engineering," *Sens. Actuators A, Phys.*, vol. 179, pp. 17–31, Jun. 2012.

[2] M. Cutkosky, R. Howe, and W. Provancher, "Force and tactile sensors," in *Handbook of Robotics*. Berlin, Germany: Springer-Verlag, 2008, pp. 455–475.

[3] N. Jamali, M. Maggiali, F. Giovanni, G. Metta, and L. Natale, "A new design of a fingertip for the iCub hand," in *Proc. IEEE/RSJ Int. Conf. Robots Syst.*, Sep. 2015, pp. 2705–2710.

[4] H. Lee, J. Chung, S. Chang, and E. Yoon, "Normal and shear forces measurement using a flexible polymer tactile sensor with embedded multiple capacitors," *J. Microelectromech. Syst.*, vol. 17, no. 4, pp. 934–942, Aug. 2008.

[5] R. S. Dahiya, L. Lorenzelli, G. Metta, and M. Valle, "POSFET devices based tactile sensing arrays," in *Proc. IEEE Int. Symp. Circuits Syst.*, May 2010, pp. 893–896.

[6] M. Ohka, H. Kobayashi, J. Takata, Y. Mitsuya, and H. Yussof, "A robotic finger equipped with an optical three-axis tactile sensor," in *Proc. Int. Conf. Robot. Autom.*, May 2008, pp. 3425–3430.

[7] *3-Axis Force Sensor Family*, accessed on Mar. 4, 2017. [Online]. Available: http://optoforce.com/3dsensor/

[8] L. Jamone, L. Natale, G. Metta, and G. Sandini, "Highly sensitive soft tactile sensors for an anthropomorphic robotic hand," *IEEE Sensors J.*, vol. 15, no. 8, pp. 4233–4426, Aug. 2015.

[9] T. P. Tomo *et al.*, "Design and characterization of a three-axis Hall effect-based soft skin sensor," *MDPI Sens.*, vol. 16, no. 4, p. 491, 2016.

[10] T. Paulino *et al.*, "Low-cost 3-axis soft tactile sensors for the human-friendly robot Vizzy," in *Proc. IEEE Int. Conf. Robot. Autom.*, Jun. 2017, pp. 967–971.

[11] M. Balicki, A. Uneri, I. Iordachita, J. Handa, P. Gehlbach, and R. Taylor, "Micro-force sensing in robot assisted membrane peeling for vitreoretinal surgery," in *Proc. Int. Conf. Med. Image Comput. Comput.-Assist. Intervention*, vol. 13. 2010, pp. 303–310.

[12] T. Keil, "Functional morphology of insect mechanoreceptors," *Microscopy Res. Tech.*, vol. 39, no. 6, pp. 506–531, 1997.

[13] Y. Tanaka *et al.*, "Demonstration of a PDMS-based bio-microactuator using cultured cardiomyocytes to drive polymer micropillars," *Lab a Chip*, vol. 6, no. 2, pp. 230–235, Jan. 2006.

[14] A. Virta, J. Timonen, R. Ras, and Q. Zhou, "Force sensing using artificial magnetic cilia," in *Proc. Int. Conf. Intell. Robots Syst.*, Oct. 2012, pp. 7–12.

[15] A. Alfadhel, B. Li, A. Zaher, O. Yassine, and J. Kosel, "A magnetic nanocomposite for biomimetic flow sensing," *Lab Chip*, vol. 14, no. 22, pp. 4362–4369, 2014.

[16] A. Alfhadel, M. A. Khan, S. Cardoso, and J. Kosel, "Magnetic tactile sensor for braille reading," *IEEE Sensors J.*, vol. 16, no. 24, pp. 8700–8705, Apr. 2016.

[17] P. Ribeiro *et al.*, "Bioinspired ciliary force sensor for robotic platforms," *IEEE Robot. Autom. Lett.*, vol. 2, no. 2, pp. 971–976, Apr. 2017.

[18] P. P. Freitas, R. Ferreira, S. Cardoso, and F. Cardoso, "Magnetoresistive sensors," *J. Phys. B, Conden. Matter*, vol. 19, pp. 165221–165242, Apr. 2007.

[19] V. Gehanno *et al.*, "Ion beam deposition of Mn-Ir spin valves," *IEEE Trans. Magn.*, vol. 35, no. 5, pp. 4361–4367, Sep. 1999.

[20] R. Ogden, *Non-linear Elastic Deformations*. North Chelmsford, MA, USA: Courier Corp., 1997.